Hindawi
International Transactions on Electrical Energy Systems
Volume 2023, Article ID 1134633, 16 pages
https://doi.org/10.1155/2023/1134633

Review Article

Performance Evaluation of Various Z-Source Inverter Topologies for PV Applications Using AI-Based MPPT Techniques

N. Kalaiarasi,[1] **A. Sivapriya**,[1] **Pradeep Vishnuram**,[1] **Mukesh Pushkarna**,[2] **Mohit Bajaj**,[3,4,5] **Hossam Kotb**,[6] **and Sadam Alphonse**[7]

[1]*Department of Electrical and Electronics Engineering, SRM Institute of Science and Technology, Kattankulathur, Tamilnadu 603203, India*
[2]*Department of Electrical Engineering, GLA University, Mathura 281406, India*
[3]*Department of Electrical Engineering, Graphic Era (Deemed to be University), Dehradun 248002, India*
[4]*Graphic Era Hill University, Dehradun 248002, India*
[5]*Applied Science Research Center, Applied Science Private University, Amman 11937, Jordan*
[6]*Department of Electrical Power and Machines, Faculty of Engineering, Alexandria University, Alexandria, Egypt*
[7]*UFD PAI, Laboratory of Analysis of Simulation and Testing, University of Ngaoundere, P.O. Box 455, Ngaoundere, Cameroon*

Correspondence should be addressed to Sadam Alphonse; ssadamalphonse@yahoo.fr

Received 4 January 2023; Revised 10 February 2023; Accepted 20 August 2023; Published 27 September 2023

Academic Editor: Lalit Chandra Saikia

Recent research has been focussed on renewable energy due to the rising need for electrical energy. Renewable energy has a low environmental impact compared to other energy sources. As a result, renewable energy sources (RESs) are the best option for generating electricity. Solar photovoltaic is one of the largest renewable power generators. Solar photovoltaic (PV) is connected to the load via power electronic converters. Most PV installations need a two-stage conversion process consisting of a boost converter to increase the load voltage and an AC-to-DC voltage source inverter to power the load. The Z-source inverter (ZSI) can confront the shortcomings of VSI and two-stage conversions. ZSI connects the PV system to the load and is used to increase the system's performance. This paper discusses the performance of various topologies of ZSI, such as traditional Z-source inverters (XZSIs); for integrating a PV source into a load, switched inductor Z-source inverters (SIZSIs) and transient Z-source inverters (TZSIs) are used. Also, artificial neural networks (ANNs), fuzzy logic controller (FLC), and adaptive neuro-fuzzy inference system (ANFIS)-based MPPT techniques are discussed for obtaining maximum power from PV panels. Based on the maximum power, the shoot-through duty ratio has been adjusted.

1. Introduction

Nowadays, solar energy plays an important part in power production. Furthermore, solar energy is accessible and generally available throughout the year. Also, it is pollution-free and does not require any fuel. On the other hand, solar energy has certain drawbacks, including lower energy conversion efficiency, greater generation costs, and strongly depending on weather conditions. A PV system contains a power converter, maximum power point controller, battery, load, or grid storage. The PV system may be connected to either an islanded or grid-connected configuration. The PV system is directly linked to the load in islanded mode, which is also known as a standalone system, whereas the PV system is interconnected to load along with the grid supply; this is known as a grid-connected mode. Inverters play a major role in the power conversion system. Single-phase and three-phase VSIs have the same qualities as classic VSI in which the output AC voltage is less than the DC input voltage. The required AC output voltage for PV and fuel cell applications is higher than the DC input voltage, necessitating the use of an additional DC-DC boost converter. This

raises the overall cost of the system and reduces its effectiveness. The inverter's switching components should not be turned on simultaneously in each phase leg. A fault current develops when both are switched on, resulting in the device malfunctioning. The ZSI overcomes the limitations of the VSI and CSI inverters. Based on the value of shoot-through duty ratio D_s, it operates either in a buck or boost mode.

1.1. Literature Review. The author Fang Zheng Peng discovered the primary topology of the classic Z-source [1, 2], which shows how the conventional ZSI confronts the obstacles and inefficiencies of the standard VSI. Because the conventional Z-source is X-shaped, it is often referred to as XZSI. In [3], a hybrid energy system that combines photovoltaic (PV) panels, fuel cells, and a single-stage grid integration system is described. The system is controlled using a Lyapunov control scheme, which ensures stability and optimizes performance. This hybrid system aims to improve the efficiency and reliability of grid integration for renewable energy sources. Figure 1 illustrates the different topologies of Z-source inverters. The Z-source inverter is distinguished primarily into transformer-based and nontransformer-based topologies.

Numerous impedance source converters have been built either by changing the standard Z-source network or by repositioning the Z-source's "L" and capacitor "C." Each topology is unique in its structure and is optimized for specific application needs. The different topologies were created to address the following constraints: reduced components of the Z-source networks, increased range of voltage gain, increased power density, and application-specific improvements. Using Z-Source converters, the authors of [4, 5] showed off several modulation strategies, including basic boost, maximum boost, and sustained boost, for a variety of power converters. The limitations of VSI and CSI are completely overcome by the essential main circuit XZSI. There are issues with the standard Z-source, such as higher voltage pressure on the capacitors and irregular supply current. Quasi-ZSI (QZSI) topology overcomes the constraints of standard ZSI. This topology is accomplished by repositioning the inductor and protection diode. The advantages of QZSI include a constant input current and a lower power rating for passive components [6–8].

In [3], the author presents an experimental study on a hybrid maximum power point tracking (MPPT) algorithm for photovoltaic (PV) grid integration. The algorithm combines two techniques, ANFIS and particle swarm optimization (PSO), to estimate MPPT under fluctuating sun irradiance. The experiment results show that the hybrid ANFIS-PSO algorithm outperforms other traditional MPPT methods in terms of efficiency and effectiveness in tracking the maximum power point of the PV system under changing solar conditions. To decrease capacitor voltage stress and restrict inrush current at the start, the next obtained architecture is an improved Z-source topology [9]. The "semi-Z-source/quasi-Z-source structure" reduces the number of active components while increasing the voltage stress on the switches compared to XZSI/QZSI. This topology avoids leakage currents while also providing a common ground for the load [10]. The incorporated Z-source design obtains a pure current directly from the supply without needing a passive filter [11, 12]. Swapping the inductor end attached to the upper and lower switches' points creates the Z-H topology. The boost operation is carried out in this topology without needing a shoot-through state or a front-end diode. In the boost mode, the equations are identical to those of a Z-source inverter [13]. The diode/capacitor-aided structure is advantageous for reducing voltage stress across the capacitor and achieving a greater voltage boost value, but it requires more components [14]. Switched inductors minimize inrush current and capacitor voltage stress but increase component count [15, 16]. In [17], a new photovoltaic power system for water-pumping applications uses a Cuk-SEPIC converter and a hybrid genetic algorithm-particle swarm optimization (GSA-PSO) maximum power point tracking (MPPT) algorithm. The system is designed to provide a reliable and efficient power source for water-pumping applications. The hybrid GSA-PSO MPPT algorithm is used to optimize the photovoltaic power system's performance and track the maximum power point of the photovoltaic panels. The study results show that the proposed system effectively provides efficient power for water pumping applications.

Generators and magnetically coupled inductors are employed to augment the voltage gain and the modulated signal in Z-source networks (M). In addition, they cut down on the number of inactive parts needed, decrease the overall price, and boost the system's power density. Figure 2 illustrates various magnetically linked or transformer-based topologies. The Y-source needs a three-winding inductor, but the T-source is best suited for neutral point-clamped converters, whereas the TZSI was developed to provide better voltage gain while maintaining reduced voltage strain on the components. It simplifies the Z-source network to a single transformer or linked inductor and a capacitor [18, 19]. The usage of ZSI in photovoltaic-based pumping applications, hybrid electric vehicles, and other applications is explored in [20, 21]. The XZSI, SIZSI, and TZSI topologies for PV applications are discussed in this chapter.

The MPPT is a method for determining the maximum power output of a photovoltaic system. In photovoltaic (PV) applications, numerous MPPT methods are employed. Numerous established strategies have been discussed in the literature, including hill climbing, incremental conductance, and P&O method. While other traditional approaches are available, the P&O technique is the most often employed. The primary disadvantages of traditional approaches are their inability to continuously track the maximum power output owing to abrupt changes in sunshine and a long trial-and-error procedure [22, 23]. In [24], an extensive practical investigation of an MPPT algorithm based on fuzzy particle swarm optimization (FPSO) control for a grid-integrated PV system is presented. The study evaluates the performance of the FPSO-based MPPT under variable operating conditions, including changes in solar irradiance, temperature, and load. In addition, the paper includes an analysis of anti-islanding protection, which is a critical aspect of grid-connected PV systems to prevent power islands and protect the grid from potential hazards. The investigation results show that the FPSO-based MPPT effectively optimizes the PV system's

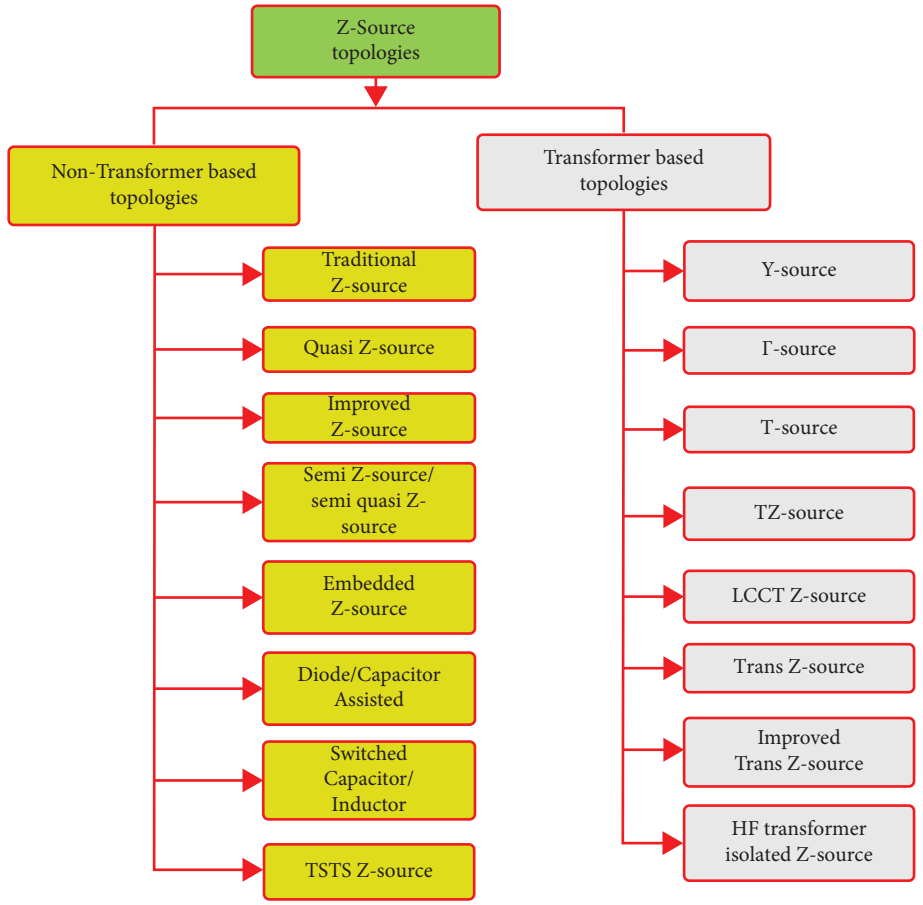

Figure 1: Various Z-source topologies used for power converters.

performance under varying operating conditions and provides reliable anti-islanding protection.

Mellit and Kalogirou discussed the challenges associated with integrating photovoltaic systems with the load which is concerned with the modeling and sizing of a PV system based on the meteorological data, as well as their simulation and control [25]. Moeed Amjad and Salam explore the soft computing methods applied to MPPT for photovoltaic applications and approaches, as well as their advantages and disadvantages. In addition, it provides ways for harmonics removal in PWM for inverter applications in renewable energy [26, 27].

ANN is optimal for integrating nonlinear input and output functions since it operates in a black-box fashion. An ANN-based MPPT with a boost converter incorporated into a PV system is described in [28, 29]. Alternatively, the fuzzy controller's fuzzy rules and membership functions are utilized to convert experimental and linguistic words to numerical values. In addition, it generates experimental output by converting raw numerical data to exploratory and linguistic concepts. In this work [30], the hardware implementation of a grid-connected photovoltaic (PV) and wind power generation system is discussed. The system uses a fuzzy particle swarm optimization (PSO) maximum power point tracking (MPPT) algorithm and a fuzzy space-vector pulse width modulation (SVPWM) inverter control to optimize the performance of the PV and wind sources. The fuzzy PSO MPPT algorithm is used to optimize the power generation from the PV and wind sources, while the fuzzy SVPWM inverter control ensures stable and efficient power conversion. The shortcoming of fuzzy computing is the inability to generate exact rules and membership functions for the specified applications because they intensely depend on past information of the system. The authors in [31–34] discus the modeling and design of an FLC-based MPPT with a boost converter for photovoltaic applications.

ANFIS combines neural networks with fuzzy logic, which is claimed to be the most important AI technology when used together. In [35, 36], an ANFIS-based MPPT is combined with a boost converter and QZSI for photovoltaic (PV) applications, and their performance metrics are evaluated. In [37], a novel MPPT system for photovoltaic (PV) systems is augmented by the Internet of Things (IoT). The system uses a modified Zeta converter and a particle swarm optimization (PSO) algorithm to optimize the performance of the PV system. The paper focuses on the hardware implementation of the proposed MPPT system and presents experimental results to validate its performance. The results show that the IoT-augmented MPPT system effectively tracks the PV system's maximum power point and has a faster convergence rate than traditional MPPT methods. According to the literature review, most

photovoltaic systems use a two-stage conversion. The drawbacks of classic VSI overcome the TZSI constraints. In addition, the SIZSI design enhances the possibility for enhancing voltage and reduces the capacitor voltage stress. The TZSI method has been developed to boost voltage and reduce the number of transformers and capacitors required in a Z-source network. The XZSI, SIZSI, and TZSI topologies are discussed in detail in this chapter. The performance of various topologies with and without a photovoltaic source is compared.

2. Topologies of Z-Source Inverter

Z-source is an LC network that is arranged in an X-shaped form. This Z-source network can be added to all power conversion circuits such as "AC-DC, DC-AC, AC-AC, DC-AC." Also, this can be used in a two-level or multilevel configuration as a voltage- or current-fed ZSI. This work mainly concentrated on the Z-source with DC-AC power conversion, which is very useful in solar PV applications. Because the PV output is inadequate for the load drive, boost converters are commonly employed to raise the magnitude of the load voltage and integrate it with the inverter to convert DC to AC, which is then linked to the load. This conversion method is known as a two-stage conversion. This factor significantly impacts the circuit's final efficiency and cost. A problem with common VSI and CSI is that their AC output voltage is always minimal or similar to the supply voltage. Short circuits with the supply due to inaccurate switching, higher system costs, and higher power dissipation are the outcomes. ZSI has been advanced in order to accomplish a one-stage conversion with buck-boost capability, overcoming the limitations of VSI and two-stage conversion. The unique property of ZSI is that it may provide VAC output that is more than the input VDC.

2.1. X-Z Source Inverter (XZSI). Figure 2(a) depicts the Z-Source arrangement, which is an "X" of inductors L1 and L2 and capacitors C1 and C2 combined with three-phase inverters. The input DC supply may be either a current or a voltage source. The output ac voltage of the three-phase XZSI may be set anywhere between 0 and 1, independently of the PV output voltage. This property demonstrates that the 3Φ XZSI is often a buck-boost inverter. The XZSI structure is examined to demonstrate the Z-source inverter's operation and control [1, 2]. There are eight possible switching states in a typical three-phase VSI. Among the eight states, six are active vectors and the remaining two are zero vectors. During active states, the load is connected to the DC source, whereas during zero states, the load terminals are short-circuited. The lower or upper three switching devices cause a short circuit at the load. However, there are "9" potential switching states in a three-phase XZSI. The three-phase XZSI has an additional zero vector along with the vectors of a regular VSI. The shoot-through zero states are responsible for the XZSI's excellent buck-boost function. This condition is the result of seven different combinations. All three legs may be combined, two legs may be combined, or one phase leg may be shot through. The load voltage at the output has been increased by allowing shoot-through mode but not allowed in VSI. The Z-source network can be made symmetrical by assuming that C1 = C2 and L1 = L2. Shoot-through (ST) and nonshoot-through (NST) states of XZSI are illustrated in Figures 2(b) and 2(c), respectively.

Figures 3(a) and 3(b) show that the line-to-line output voltage V_{ab} without a filter is 500 V for the input of 150 V. So, the boost factor is approximately 3.4. The current and voltage stresses of upper and lower switching devices are given in Figure 3(b). The value of the shoot-through duty cycle (D_{sh}) for the XZSI circuit is restricted from 0 to 0.5. During low input DC voltage, a larger value of "D_{sh}" is required to boost the output voltage in practical uses where the sources are PV and fuel cells. This implies that the Z-source inverter has been in a shoot-through zero condition for a prolonged period of time. According to the relationship $M = (1 - D_{sh})$, the modulation index is reduced to the lower level for a higher value of D_{sh}, resulting in inadequate inversion capability at the fundamental frequency. As a result of the excessive THD, the output performance suffers dramatically. The value of M should be kept as close to 1 as possible for optimal design. This shortcoming is overcome by SIZSI.

2.2. Switched Inductor ZSI. A SIZSI has been created by incorporating the idea of a switched inductor into the Z-source configuration. This architecture is used to increase voltage flexibility, and a short shoot-through time (D_{sh}) is necessary to give an improved voltage conversion ratio, which is helpful in improving the power quality of the inverter. In comparison to the XZSI, SIZSI has a better voltage gain modulation index. In addition to XZSI components, 6 diodes and 2 inductors are included in the SIZSI circuit. Figure 4(a) represents the circuit diagram of SIZSI, and Figures 4(b) and 4(c) show the corresponding equivalent circuit of SIZSI in ST and NST state, respectively. The top switched inductor cell is on the path of "L1-L2-D2-D3-D5," while the bottom cell is on the path of "L3-L4-D1-D4-D6." The DC bus obtains energy from the capacitor through the SL cell. The design equations are as followed in [15]. From Figure 5(a), the output voltage is 500 V with a supply voltage of 150 V. According to Figures 3(a) and 5(a), the XZSI delivers 220 V, the SIZSI offers 240 V, and the inrush current is discontinuous. Further improving the inrush current TZSI topology has been discussed in Section 2.3. Figure 5(b) shows the voltage stress and current stresses on the switches in SIZSI.

2.3. Trans Z Source Inverter (TZSI). In contrast to XZSI, which has two inductors and two capacitors, the TZSI only has one transformer and one capacitor. The TZSI is depicted in Figure 6(a), and its corresponding equivalent circuit in the ST state and NST state is shown in Figures 6(b) and 6(c), respectively. It offers a larger voltage inversion capability, reduced voltage stress, continuous inrush current, and lower Z-source network component ratio. The TZSI is capable of reducing the high inrush current during start-up. The two inductors in ZSN are exchanged with a transformer to

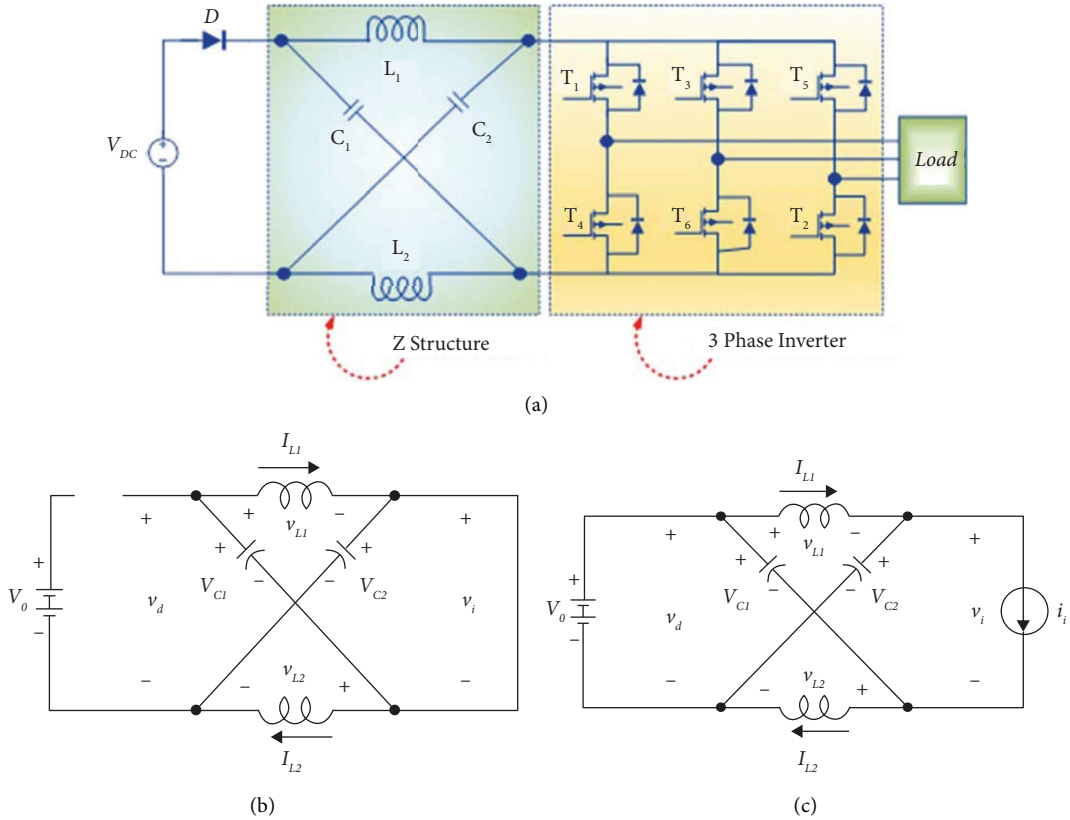

Figure 2: (a) Circuit diagram of XZSI. (b) ST state of XZSI. (c) NST state of XZSI.

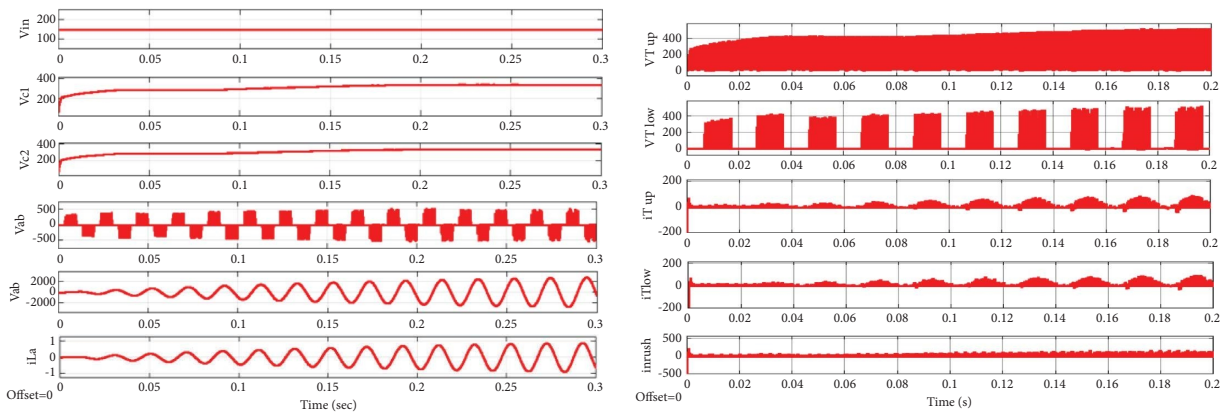

Figure 3: (a) Output waveforms of XZSI. (b) Voltage stress and current stresses on the switches in XZSI.

improve the voltage gain; this structure is known as TZSI. High boost voltage gain is produced by varying the transformer turn ratio. In this topology, inrush current is suppressed by using a single inductor and capacitor [18].

The output waveforms and switching stress of TZSI are deployed in Figures 7(a) and 7(b), and the switching stress on the switches is around 280 V, as seen in these waveforms. In comparison to SIZSI, the capacitor voltage has been reduced to 80 V. Furthermore, the topologies discussed in Section 2 have been integrated into PV, and AI-based MPPT techniques are discussed in Section 3.

3. MPPT Techniques Using AI

MPPT is a technique for determining the maximum power output from RES such as PV and wind energy systems. Mechanical tracking and electronic tracking are subcategories of MPPT. When a solar panel is mounted without a tracking device, it receives only around 20% to 30% of the energy it generates, most of which is dissipated as heat. The panel is rotated according to the sun's direction in mechanical tracking to increase power generation. The moveable tracking system comprises a control circuit, an amplifier, a driving

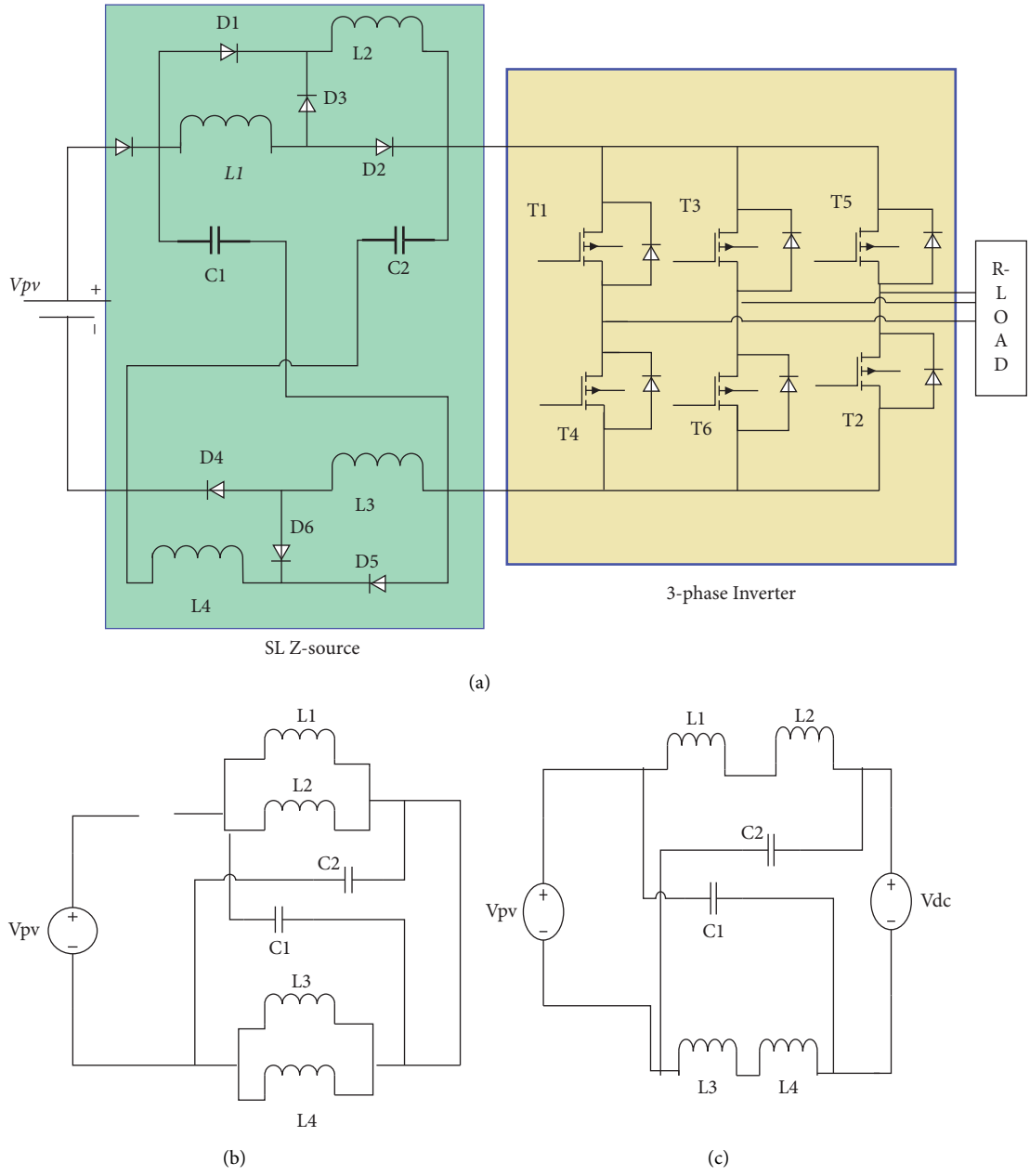

Figure 4: (a) Circuit diagram of SIZSI. (b) SIZSI during ST state. (c) SIZSI during NST state.

circuit, and a geared motor. Along with this tracking, the photovoltaic system consists of a number of photovoltaic panels, a DC-DC converter, an inverter, and a battery. Consequently, the converter utilizes the DC voltage produced by the PV panel as its input. The stepper motor drive and converter drive circuits receive pulses from the control circuit. Movable tracking is useful for lower-level power production but unsuitable for higher-level power generation because the gear motor and other circuits utilize a large amount of generated power. Electronic tracking is used to overcome this problem. Mechanical tracking requires that the PV panel be rotated to achieve maximum power, while electronic tracking requires that the PV panel be operated in the maximum power point region of the PV characteristics.

Perturb & Observe (P&O), Incremental Conductance (Inc-Cond), Hill climbing (HC), and AI-based MPPT algorithms are some of the electronic tracking methods that can be used. Among the above methods, P&O, Inc-Cond, and HC are conventional methods that do not work for sudden changes in weather conditions. To overcome these limitations, AI-based algorithms are preferred.

3.1. ANN-Based MPPT Technique. Artificial neural network algorithms are powerful data modeling tools for describing complicated input/output relationships. They function similarly to the human brain. It is a simple prediction algorithm that attempts to replicate the link between input and

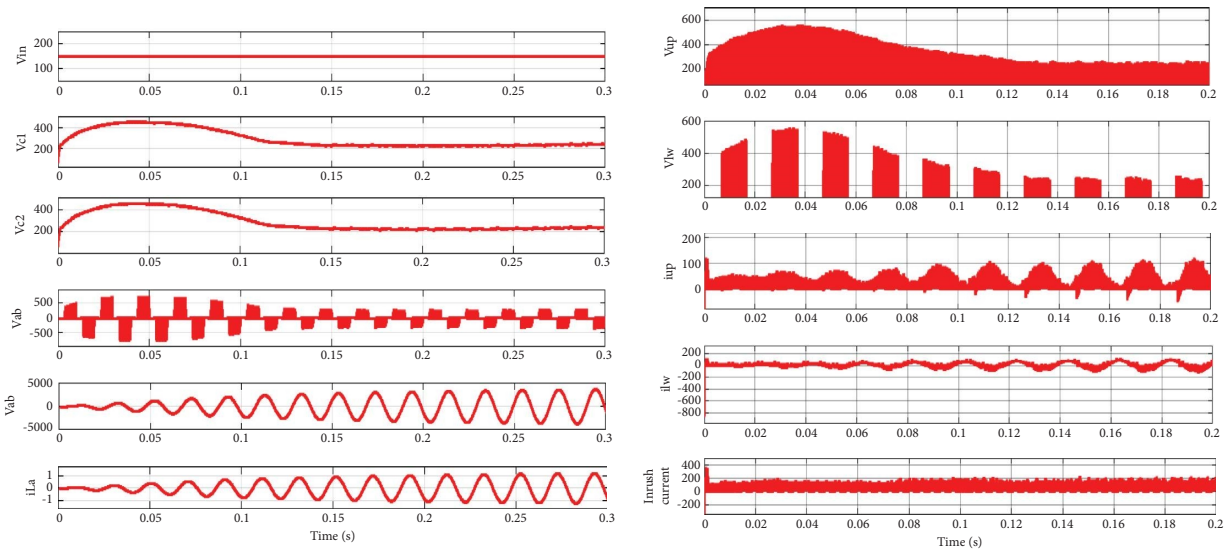

(a) (b)

Figure 5: (a) Output waveforms of SIZSI. (b) Voltage stress and current stresses on the switches in SIZSI.

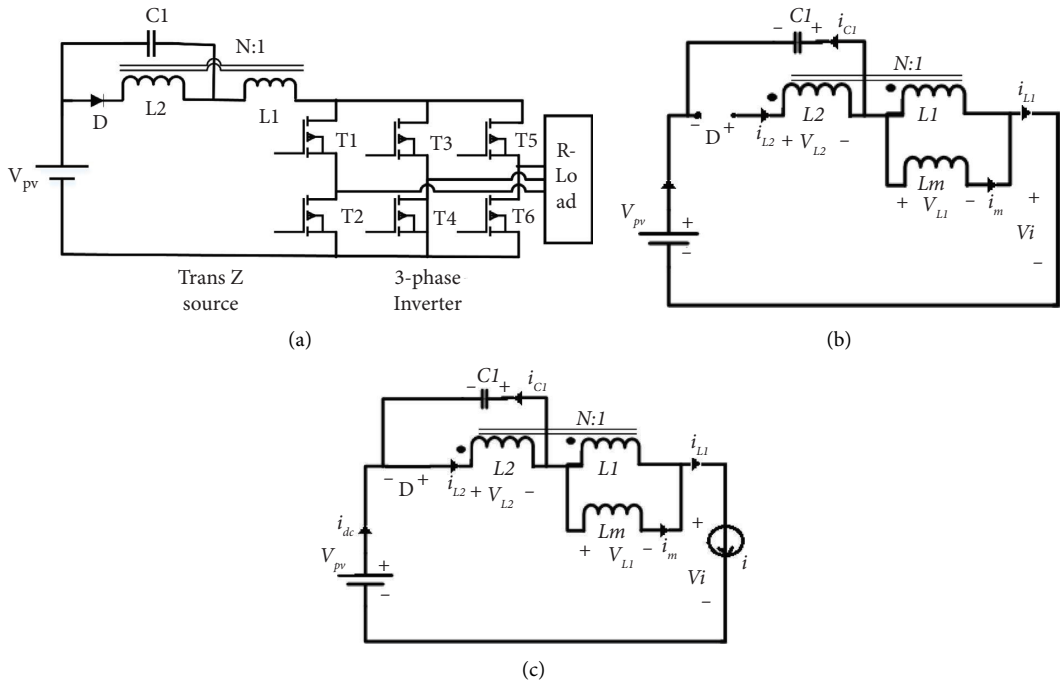

Figure 6: (a) Circuit diagram of TZSI. (b) TZSI during ST state. (c) NST state.

output variables. Any nonlinear function can be implemented with ANN by repeatedly training from historical input once the required accuracy has been achieved. The ANN has a fully connected neural network structure, which can do complex perceptual and reorganizational tasks far more quickly than even today's most common high-performance computers. A neural network's input and output nodes are equal in number to the number of inputs and outputs to the network, respectively. It is a matter of trial and error to figure out how many secret levels there are and how many nodes are in each. The "Levenberg–Marquardt" optimization technique is employed in this study to train ANN. The NN output is MPP voltage, which is determined by irradiance and temperature input variables.

A network with structure 2-10-1 is used in the ANN-based MPP tracking. Irradiance and temperature are the network's two inputs, whereas the MPP voltage of PV is the output. 220 datasets from a MATLAB simulation were employed to train the neural network. The MATLAB-NN fitting tool was utilized by mapping the inputs to the targets

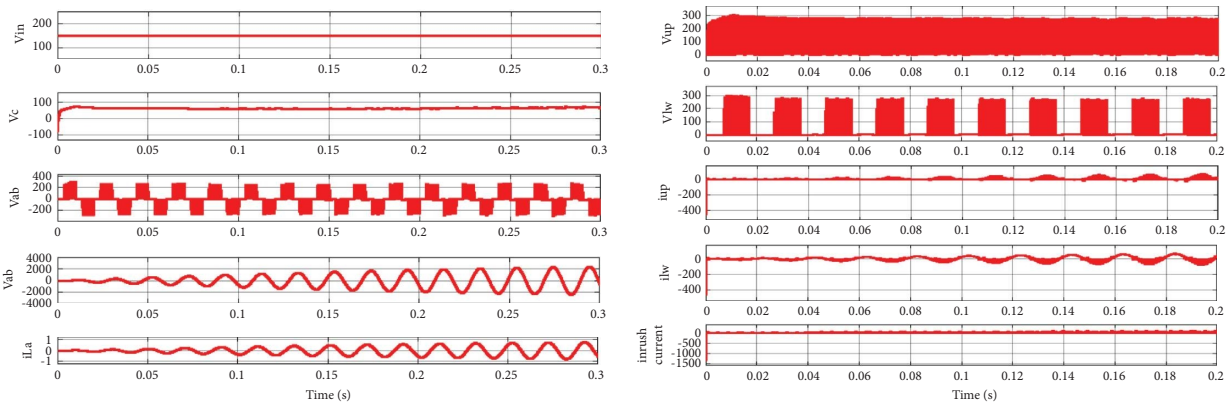

(a) (b)

Figure 7: (a) Output waveforms of trans ZSI. (b) Effects of voltage and current on the switches capacitor in TZSI.

to realize the required nonlinear function. The fitting tool specifies the structure of ANN, which is then trained using training data. The network structure is changed randomly until the fitting tool achieves the required accuracy. The means square error (MSE) for various iterations is determined by the performance curve. The performance curve shown in Figure 8 shows that optimal error values are assessed for training, validation, and testing above 100 iterations.

The performance graph illustrates the mapping of targeted values vs. trained values. The neural network is trained when the maximum data are on the plot fit line. R is 0.9999 in all three scenarios, i.e., training, validation, and testing regression. This means that the network has been trained. The target values for testing new inputs are computed from the PV module Simulink diagram. The target values are denoted by (A), while the values produced by the neural network are denoted by (B). The proportion of errors ranges from 0.09% to 4.41%. NN is integrated with PV and Z-Source inverters after training and testing. The performance of XZSI, SIZSI, and TZSI is verified by integrating with ANN. Figure 9 depicts the voltage output of the aforementioned topologies.

ANN-based MPPT calculates the output voltage from this waveform, with XZSI producing 200 V, SIZSI producing 210 V, and TZSI producing 180 V. Consequently, SIZSI provides more benefit. Because the neural network acts as a black box, it lacks investigative sense. Fuzzy controllers are used to monitor MPP voltage to compensate for this shortcoming.

3.2. FLC-Based MPPT Technique. Fuzzy controllers deal with indeterminate inputs and do not need any mathematical formulae to handle nonlinearities. Fuzzy-based controllers are built in three steps: fuzzification, rule basis, and defuzzification. During the fuzzification process, numerical input variables are turned into linguistic labels using the membership function (MF), as shown in Figures 10(a) and 10(b). Low, medium, and high are the types of linguistic labels utilized. An inference engine tool

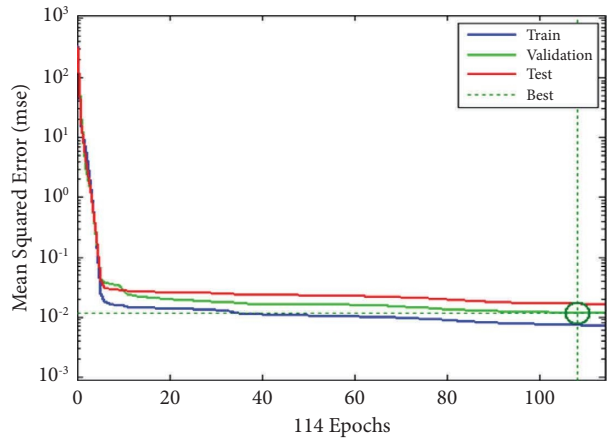

Figure 8: Performance of NN during training.

provides a logical conclusion based on a fuzzy rule and transforms the fuzzy sets into linguistic outputs. MF is used in defuzzification to convert the fuzzy controller's output from a linguistic label to a numerical variable. Fuzzy controllers have been shown to work effectively under unpredictably changing atmospheric conditions. The user's familiarity, the exact error computation, and turning up with the rule basis may all be used to establish their effectiveness. FLC is a good tool for modeling nonlinear control systems, such as MPP tracking for PV systems. Irradiance, temperature errors, and error changes are signals that are fed into the fuzzy controller. The outcome of FLC is V_{MPP}, which has been used to estimate the shoot-through-duty ratio. The modulation index (M) is derived from this duty ratio and applied to the ZSI triggering circuit. The fuzzy controller's output has a larger incremental reference voltage to make the system more responsive during transients. At the top of the PV curve, however, there are zero references, which help to reduce oscillations. The input and output membership functions are meant to reflect the PV output graph's asymmetrical natural surroundings. Membership functions are deeper at the midpoint to provide greater compassion in the MPP

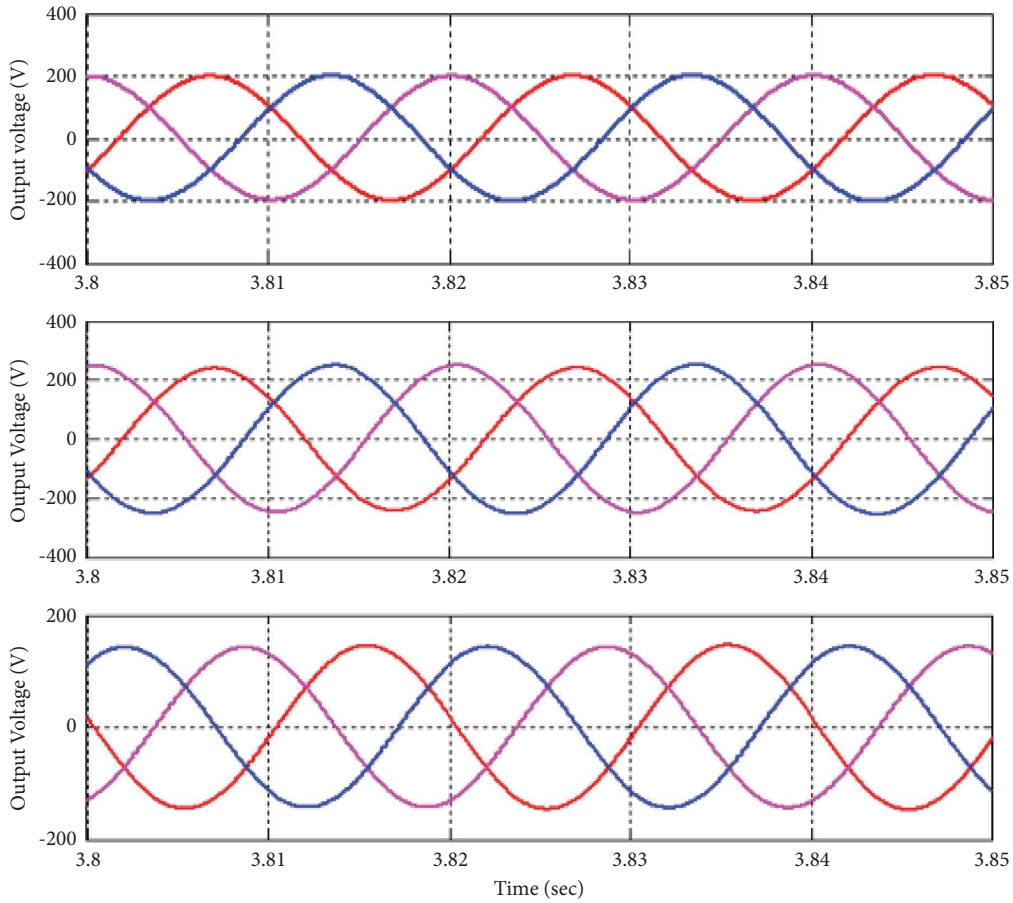

Figure 9: ANN-based MPPT output voltage for XZSI, SIZSI, and TZSI.

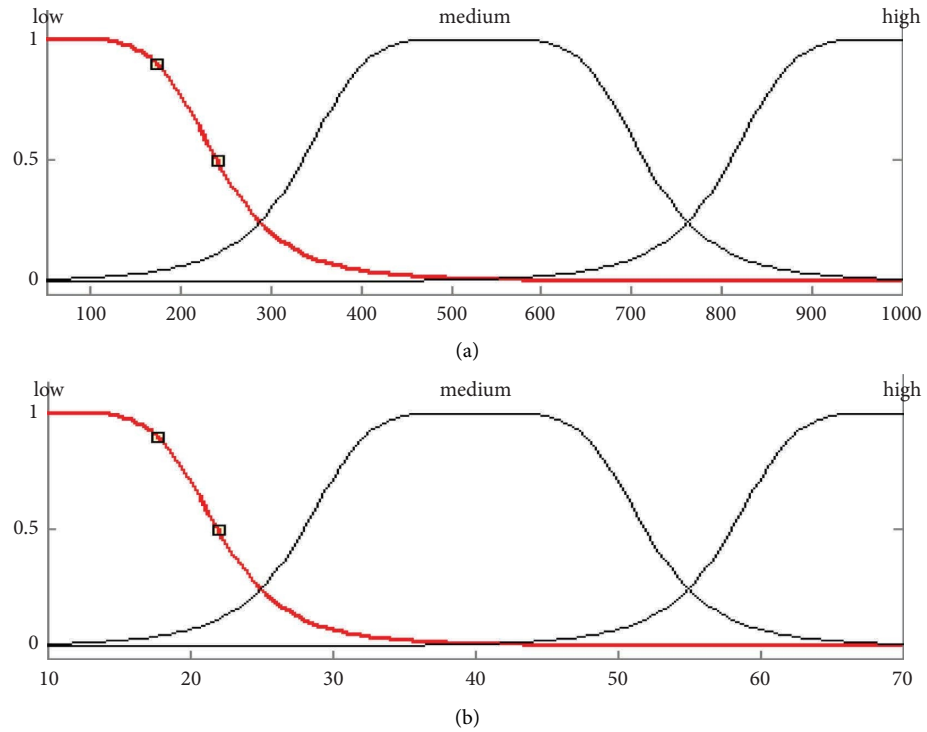

Figure 10: Membership function for (a) irradiance and (b) temperature.

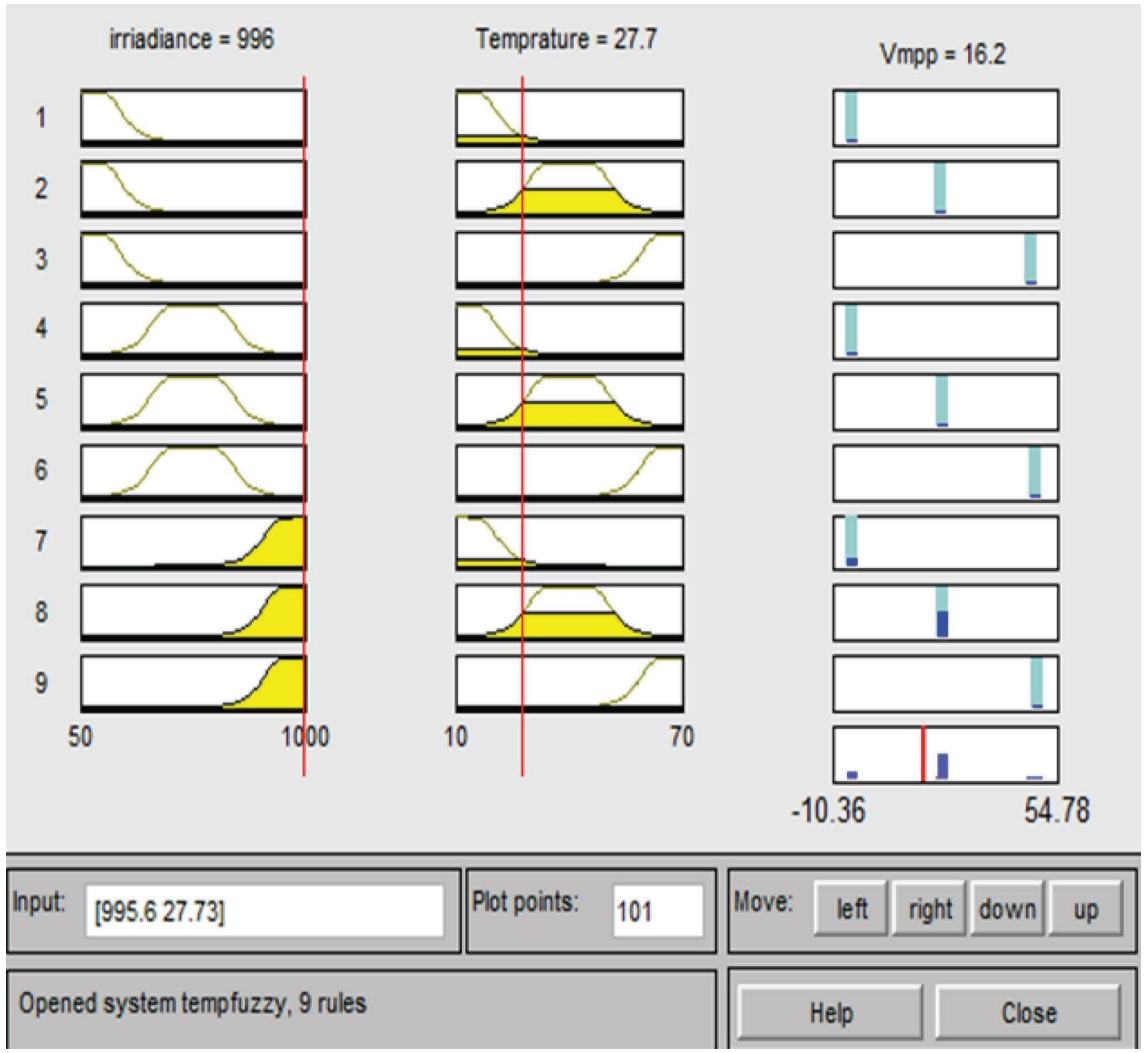

Figure 11: Rule viewer for FLC controller.

area. The input values correlate to the proper reference frame using normalized input membership functions with suitable fine-tuning parameters.

Nine rules are formed for three linguistic labels. Reducing the linguistic labels of inputs and output functions decreases the rules but also decreases the output accuracy. The inference mechanism governs the fuzzy controller's output. The Sugeno inference approach and max-min composition are employed to calculate the output in this study. This approach is more computationally efficient and has better interpolative features than previous implication function-based methods. As a result, the Sugeno inference approach is widely used in most engineering applications. The rule viewer for the Sugeno model is shown in Figure 11. MATLAB's fuzzy block is built using the input and output information. The fuzzy block is combined with the photovoltaic, ZSI, and load. All three topologies presented in Section 3 have fuzzy-based MPPT implemented. Figure 12 shows the output voltage of fuzzy-based MPPTs with various topologies, and it can be shown that XZSI generated 210 V, SIZSI produced 230 V, and TZSI produced 140 V.

The rules and membership function, which are dependent on the system's past knowledge, are the limitations of fuzzy controllers. Because ANFIS integrates both fuzzy and ANN controllers, the downfalls of both fuzzy and ANN controllers are eliminated.

3.3. ANFIS-Based MPPT. There were 220 input/output data sets used to train the ANFIS. These results were obtained by using the MATLAB Simulink tool to change the irradiance from 50 W/m^2 to 1000 W/m^2 at 50 W/m^2 intervals and the working temperature from 10°C to 70°C at 6°C intervals. The MATLAB toolbox is used to conduct the training in an offline setting over the course of 30,000 epochs. As a result of the training process, a five-layer neuro-fuzzy architecture is produced. The inputs are irradiance and temperature, which are then translated to appropriate membership functions, each of which has three linguistic labels. It generates membership functions based on previous knowledge obtained from training data. For training, an aggregate of 220 data sets is used, and nine fuzzy rules are chosen. The Genfis 1 command in MATLAB is used to construct a hybrid

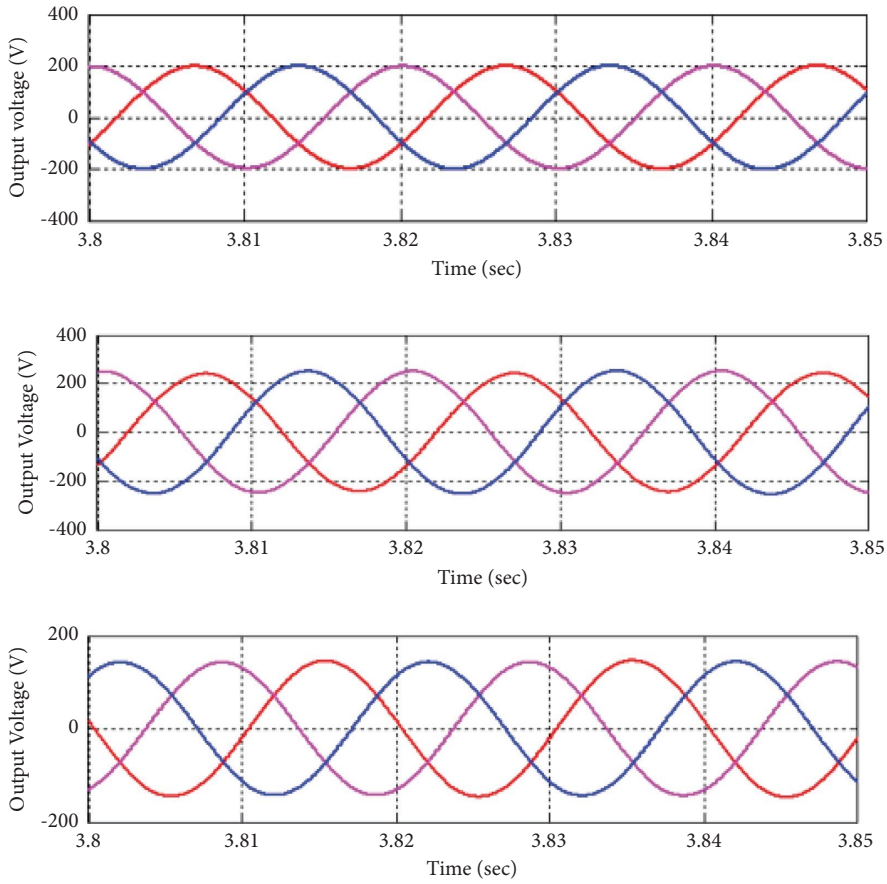

Figure 12: Output voltage of XZSI, SIZSI, and TZSI for FLC-based MPPT.

learning algorithm that recognizes the parameters of Sugeno-type fuzzy inference systems. Figure 13 depicts the ANFIS structure that was produced. Bell membership functions for "nine" rules are presented in the rule viewer shown in Figure 14, which corresponds to the provided ANFIS structure.

Several MFs, including Gauss, trapezoidal, and Bell MF with 9 rules, are used to train the ANFIS structure. Table 1 displays the error values and MPP voltage achieved for the aforementioned membership functions with 30000 epochs. In terms of accuracy and MPP voltage, the bell MF surpasses the others. Hence, bell MF is chosen; further fixing the number of rules, the ANFIS network is tested using the next minimal $(2 * 2 = 4)$ rules which are verified with two membership values "low" and "high," and the results are checked to determine the number of rules. V_{mpp} obtained for four rules is 16.6 V, whereas V_{mpp} obtained for nine rules is 17.1 V. At STC, the calculated voltage value V_{mpp} from the neural network controller is 16.96 V. Since neural networks produce low MPP voltage, an ANFIS with a bell membership function and nine rules produces high MPP voltage. Hence, examining each model independently has chosen an optimal one for prediction. One of the most important performance criteria is the model's tracking efficiency. All three of the ZSI topologies covered in Section 3 are incorporated into the ANFIS-based MPPT shown in Figure 15, which displays the output voltage and inrush current waveform. According to Figure 15, XZSI delivers 220 V, SIZSI offers 240 V, and TZSI provides 140 V. XZSI and SIZSI create discontinuous inrush current, but TZSI produces a very low value of continuous inrush current (1.4 A). Based on the above discussion, the results show that ANFIS-based MPPT with SIZSI produces greater output voltage than the other topologies, whereas TZSI-based ANFIS MPPT generates a constant low inrush current. Figure 16 depicts the load voltage, load current, power, and duty cycle of an XZSI based on an ANFIS.

Table 2 compares AI-based MPPT performance with three ZSI topologies. The table shows that ANFIS with SIZSI is ideal for high-gain processes while ANFIS with TZSI is desired for low starting current and capacitor voltage strain, as mentioned in Section 3.3.

3.4. Real-Time Implementation of Proposed Technique. This section addresses the use of the dspace DS1104 to implement a suggested approach on real-time hardware. The connection between the MATLAB/SIMULINK model and the actual inverter hardware is facilitated by the dspace DS1104, as shown in Figure 17. Sensors are utilized to sense the signals from the input system. The dspace block provides the control signal and generates the switching pulses through the driver circuit. The resulting SPWM signals are

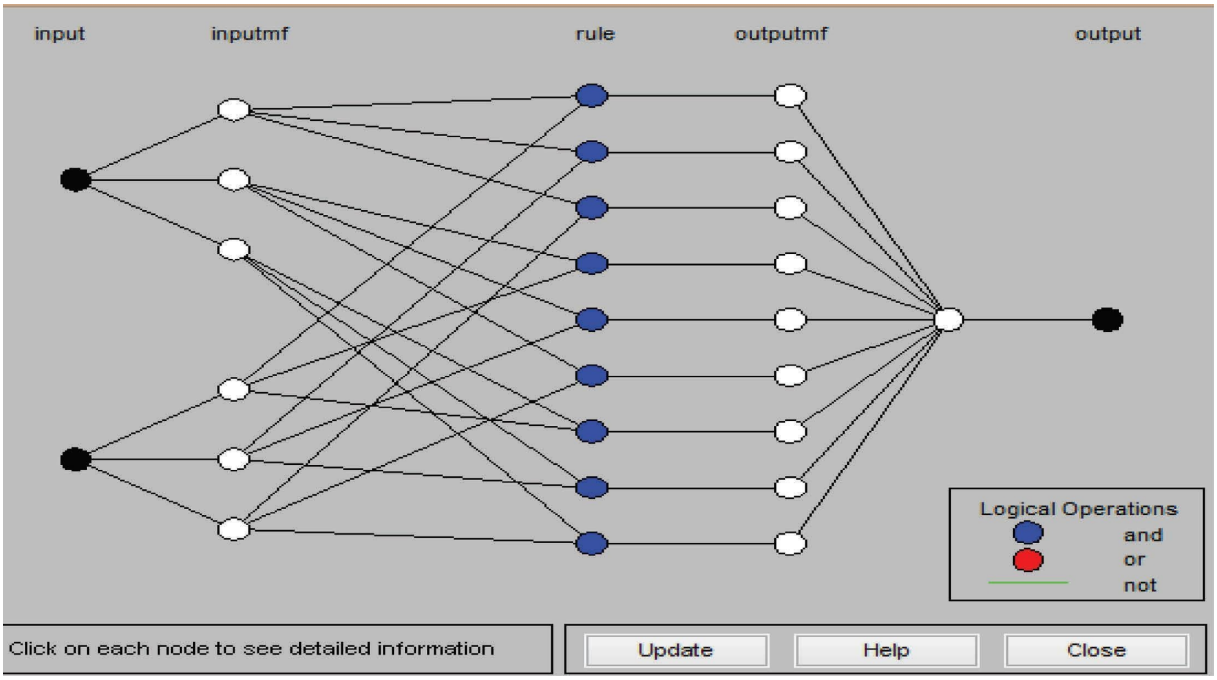

Figure 13: Framework of the ANFIS model.

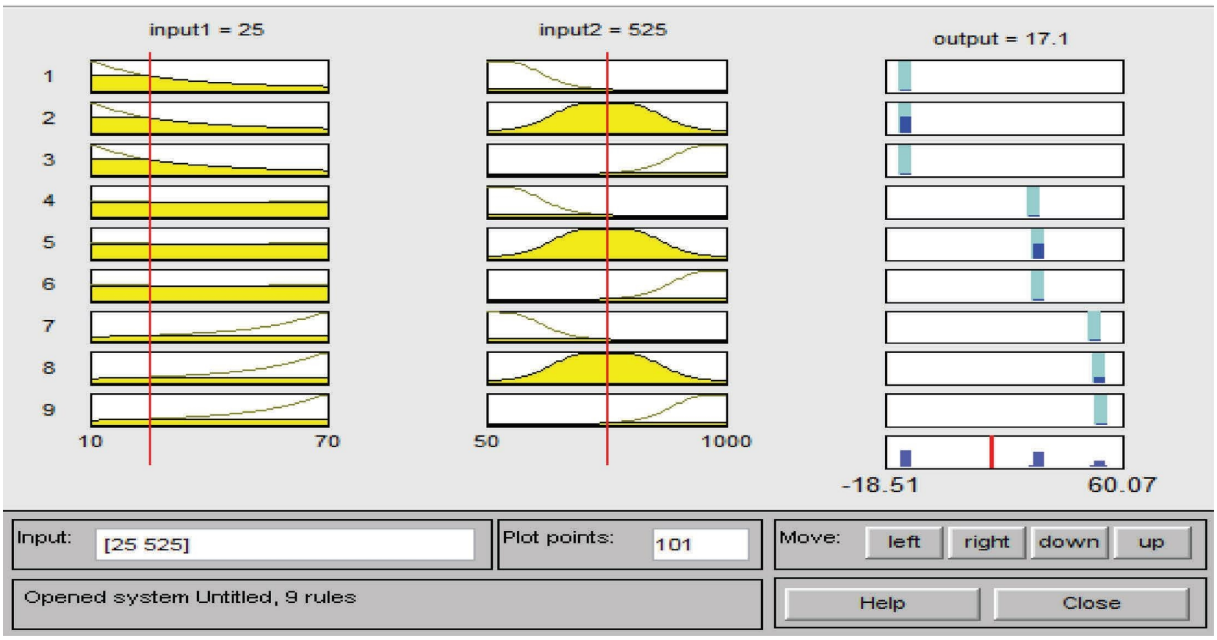

Figure 14: ANFIS structure bell MF rule viewer for 9 rules.

Table 1: Selection of membership function.

Type of membership function	Error value	MPP voltage (V_{mpp}) (V)
Gauss (with 9 rules)	0.1332	16.9
Trapezoidal (with 9 rules)	0.1896	16.9
Bell (with 9 rules)	0.1139	17.1
Bell (with 4 rules)	0.2580	16.6

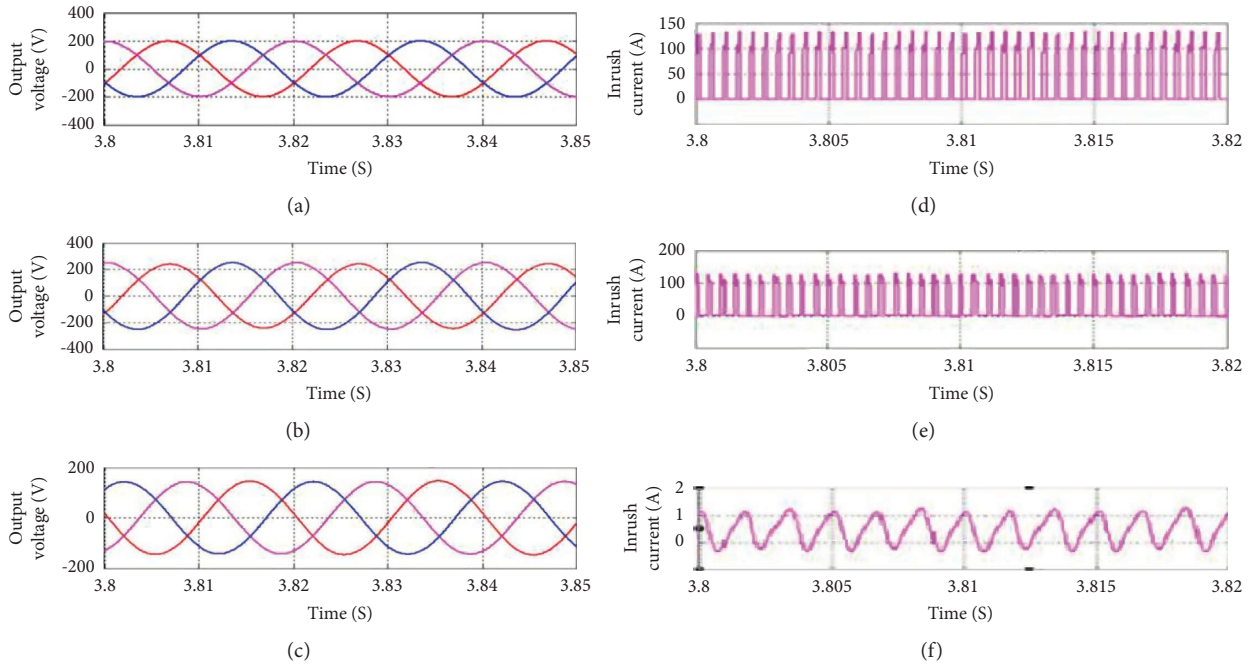

Figure 15: Output voltage of ANFIS-based MPPT with (a) XZSI, (b) SIZSI, and (c) TZSI; inrush current of ANFIS-based MPPT with (d) XZSI, (e) SIZSI, and (f) TZSI.

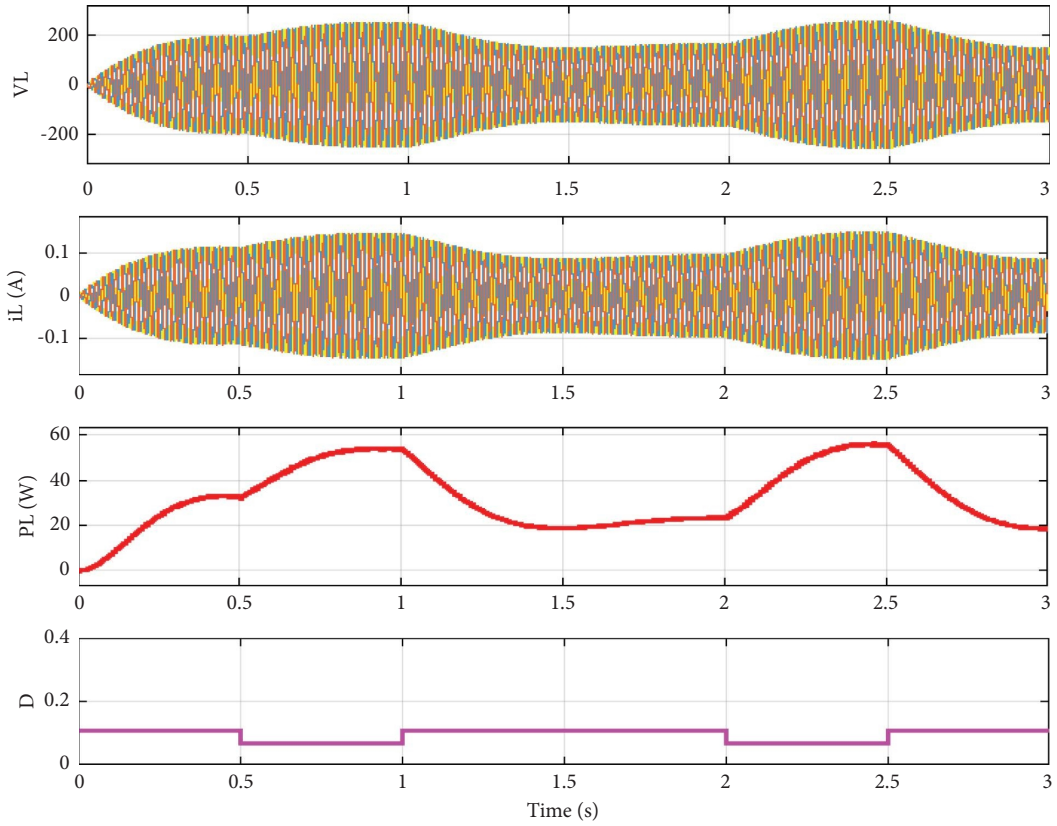

Figure 16: Load voltage waveforms of ANFIS-based MPPT with XZSI topology.

Table 2: AI-based MPPT performance with various ZSI topologies.

Performance parameters	MPPT using ANN			MPPT using FLC			MPPT using ANFIS		
Topology type	XZSI	SIZSI	TZSI	XZSI	SIZSI	TZSI	XZSI	SIZSI	TZSI
Output voltage	200 V	210 V	180 V	210 V	230 V	140 V	210 V	240 V	140 V
Inrush current	145 A	100 A	1.4 A	140 A	110 A	1.3 A	135 A	100 A	1.2 A
THD in %	0.62	0.82	0.2	0.83	0.93	0.19	0.8	0.93	0.15
D_{sh} value	0.24	0.2	0.18	0.29	0.24	0.19	0.29	0.24	0.19
MI	0.76	0.80	0.82	0.71	0.76	0.81	0.71	0.76	0.81
Input current	DM	DM	CM	DM	DM	CM	DM	DM	CM

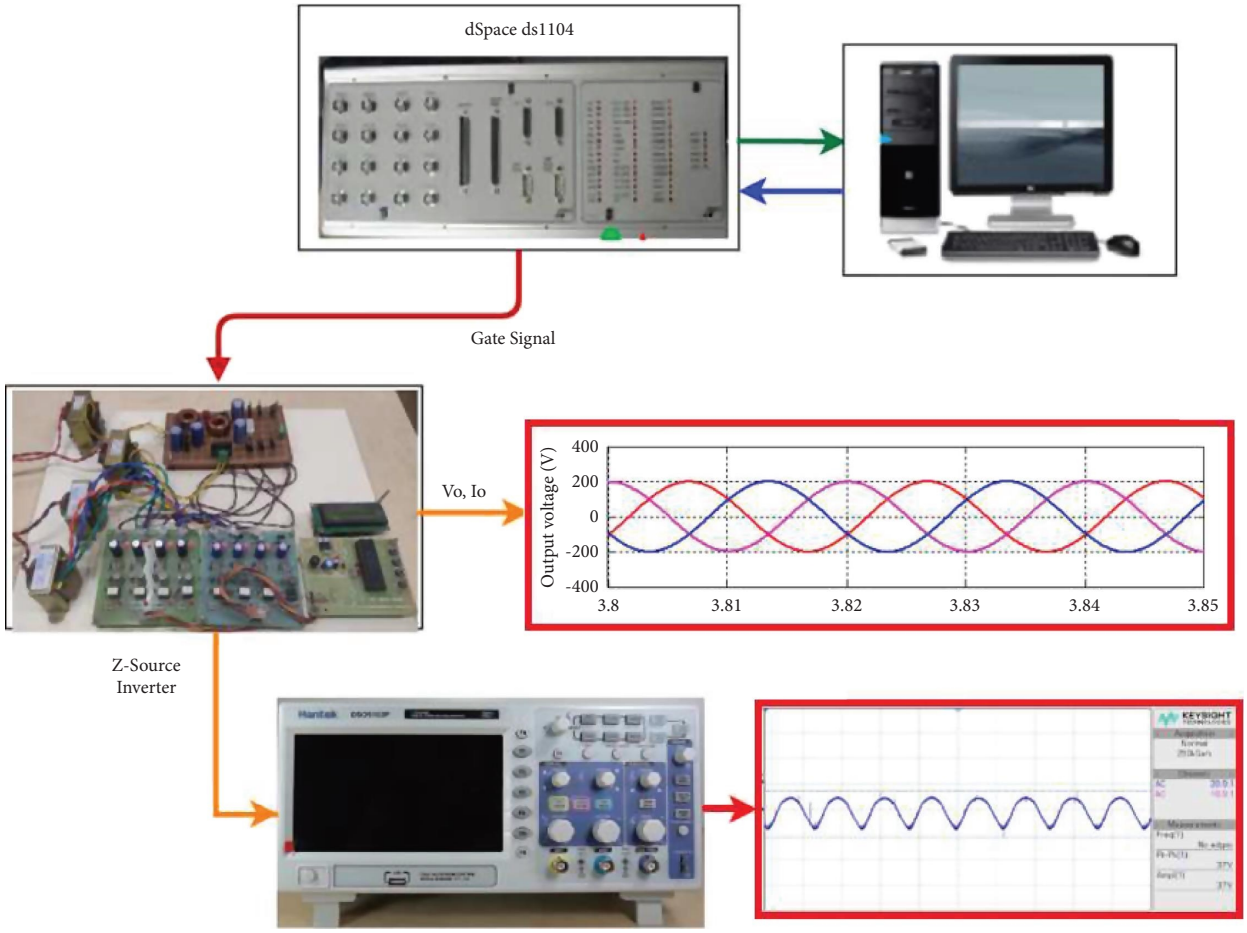

Figure 17: Experimental setup for ZSI.

then connected to the inverter's hardware, which is operated under load and monitored using an oscilloscope with digital storage. Figure 18 displays the PWM signal from the dspace controller, while Figure 19 shows the voltage across the load.

The benefits of using this AI-based MPPT technique include increased efficiency in solar energy systems, improved performance of photovoltaic systems, cost savings, and enhanced integration of renewable energy.

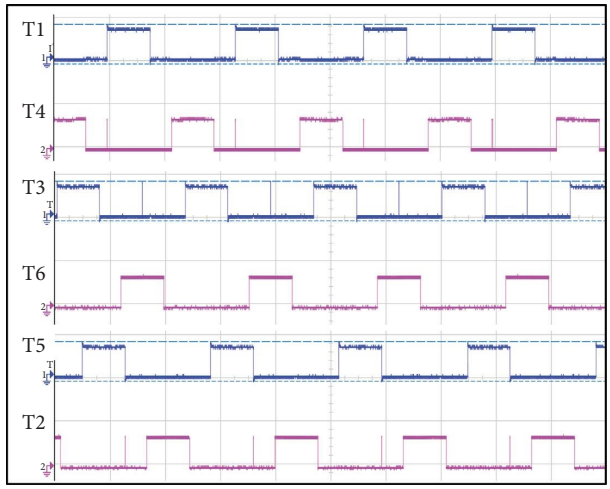

Figure 18: PWM pulse from DSpace.

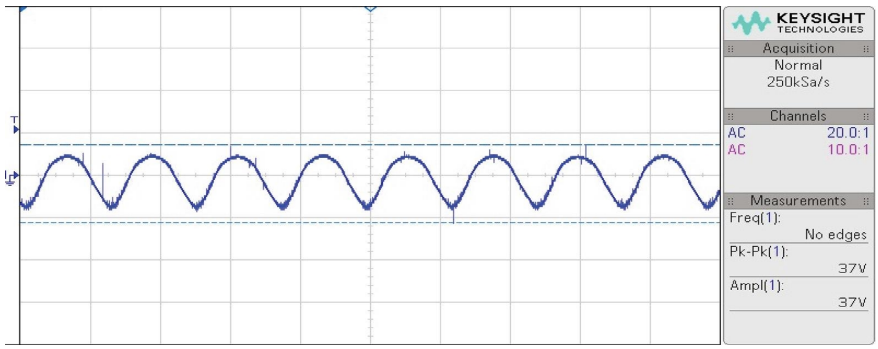

Figure 19: Output voltage of ZSI.

4. Conclusion

The selection of power converters is crucial for PV load integration. Typically, the output power of PV is inadequate to power the demand. Consequently, a boost converter is installed among the photovoltaic and VSI. These arrangements enabled double-stage energy conversion. As a result of an increasing number of switching devices, losses also increase. By substituting VSI with ZSI, these limitations of VSI can be addressed. SIZSI and TZSI topologies are chosen among the several ZSI topologies available. The capacitor's voltage stress is reduced from 330 V to 200 V using SIZSI compared to ordinary ZSI, and switching stress is reduced to 250 V. Also, the capacitor voltage stress in TZSI has been reduced to 80 V, which is less than SIZSI. Therefore, the TZSI architecture is beneficial for capacitor voltage stress as well as high input current. Furthermore, MPPT algorithms are necessary to acquire the maximum power when these inverters are evaluated with a photovoltaic system. The traditional MPPT algorithm P&O was compared to AI-based MPPT techniques such as ANN, FUZZY, ANFIS, and PSO. This leads to the conclusion that the PSO-based MPPT outperforms the P&O technique in terms of tracking time and oscillations. Furthermore, the performance characteristics of ANFIS are superior to those of ANN and fuzzy with an improvement in the efficiency of 96.8% and an RMSE of 0.02.

Data Availability

Data are available on request to the corresponding author.

Conflicts of Interest

The authors declare that they have no conflicts of interest.

References

[1] N. Subhani and R. Kannan, "Z-source inverter topologies with switched Z-impedance networks: a review," *IET Power Electronics*, vol. 14, no. 4, pp. 727–750, 2021.

[2] M. K. Nguyen and Y. O. Choi, "Maximum boost control method for single-phase quasi-switched-boost and quasi-Z-source inverters," *Energies*, vol. 10, no. 4, p. 553, 2017.

[3] N. Priyadarshi, "An experimental estimation of hybrid ANFIS–PSO-based MPPT for PV grid integration under fluctuating sun irradiance," *IEEE Systems Journal*, vol. 14, no. 1, pp. 1218–1229, 2020.

[4] Y. P. Siwakoti, "New magnetically coupled impedance (Z-) source networks," *IEEE Transactions on Power Electronics*, vol. 31, no. 11, pp. 7419–7435, 2016.

[5] Z. Chen, Y. Chen, and B. Zhang, "An equivalent voltage source placement rule for impedance source network and performance assessment," *IEEE Transactions on Industrial Electronics*, vol. 65, no. 10, pp. 8382–8392, 2018.

[6] R. Seyezhai, K. Abinaya, V. Akshaya, and U. Induja, "Simulation, analysis and development of PV fed quasi impedance source inverter," *International Journal of Electrical and Electronics*, vol. 3, pp. 201–212, 2013.

[7] D. Sun, B. Ge, D. Bi, and F. Z. Peng, "Analysis and control of quasi-Z source inverter with battery for grid-connected PV system," *International Journal of Electrical Power and Energy Systems*, vol. 46, pp. 234–240, 2013.

[8] B. Ge, H. Abu-Rub, F. Z. Peng et al., "An energy-stored quasi-Z-source inverter for application to photovoltaic power system," *IEEE Transactions on Industrial Electronics*, vol. 60, no. 10, pp. 4468–4481, 2013.

[9] Y. Tang, S. Xie, and C. Zhang, "An improved Z-Source inverter," *IEEE Transactions on Power Electronics*, vol. 26, no. 12, pp. 3865–3868, 2011.

[10] D. Cao, S. Jiang, X. Yu, and F. Z. Peng, "Low cost Semi-Z-source inverter for single phase photovoltaic systems," *IEEE Transactions on Power Electronics*, vol. 26, no. 12, pp. 3514–3523, 2011.

[11] F. Gao, P. C. Loh, D. Li, and F. Blaabjerg, "Asymmetrical and symmetrical embedded Z-source inverters," *IET Power Electronics*, vol. 4, no. 2, pp. 181–193, 2011.

[12] P. C. loh, F. Gao, and F. Blabbjerg, "Embedded Z-source inverter," *IEEE Transactions on Industry Applications*, vol. 46, no. 1, pp. 256–267, 2010.

[13] A. Taghieh, C. Zhang, and K. A. Alattas, "A predictive type-3 fuzzy control for underactuated surface vehicles," *Ocean Engineering*, vol. 266, no. 2022, Article ID 113014, 2022.

[14] C. J. Gajanayake, F. L. Luo, H. B. Gooi, P. L. so, and L. K. siow, "Extended-boost Z-Source inverters," *IEEE Transactions on Power Electronics*, vol. 25, no. 10, pp. 2642–2652, 2010.

[15] M. Zhu, Y. Kun, and F. L. Luo, "Switched inductor Z-source inverter," *IEEE Transactions on Power Electronics*, vol. 25, no. 8, pp. 2150–2158, 2010.

[16] M. K. Nguyen, Y. C. Lim, and J. H. Choi, "Two switched-inductor quasi-Z-source inverters," *IET Power Electronics*, vol. 5, no. 7, pp. 1017–1025, 2012.

[17] N. Priyadarshi, M. S. Bhaskar, S. Padmanaban, F. Blaabjerg, and F. Azam, "New CUK-SEPIC converter based photovoltaic power system with hybrid GSA-PSO algorithm employing MPPT for water pumping applications," *IET Power Electronics*, vol. 13, no. 13, pp. 2824–2830, 2020.

[18] W. Qian, F. Z. Peng, and H. Cha, "Trans-Z-source inverters," *IEEE Transactions on Power Electronics*, vol. 26, no. 12, pp. 3453–3463, 2011.

[19] M.-K. Nguyen, Y.-C. Lim, and S.-J. Park, "Improved trans-Z-source inverter with continuous input current and boost inversion capability," *IEEE Transactions on Power Electronics*, vol. 28, no. 10, pp. 4500–4510, 2013.

[20] Q. Liao, S. Li, F. Xi et al., "High-performance silicon carbon anodes based on value-added recycling strategy of end-of-life photovoltaic modules," *Energy*, vol. 281, no. 2023, Article ID 128345, 2023.

[21] S. Jain, C. Ramulu, S. Padmanaban, J. O. Ojo, and A. H. Ertas, "Dual MPPT algorithm for dual PV source fed open-end winding induction motor drive for pumping application," *Engineering Science and Technology, an International Journal*, vol. 19, no. 4, pp. 1771–1780, 2016.

[22] A. Reza Reisi and M. Hassan Moradi, "Classification and comparison of maximum power point tracking techniques for photovoltaic system: a review," *Renewable and Sustainable Energy Reviews*, vol. 19, pp. 433–443, 2013.

[23] X. Ma, Y. Wan, Y. Wang et al., "Multi-Parameter practical stability region analysis of wind power system based on limit cycle amplitude tracing," *IEEE Transactions on Energy Conversion*, pp. 1–13, 2023.

[24] X. Lin, R. Yu, J. Yu, and H. Wen, "Constant coupling effect-based PLL for synchronization stability enhancement of grid-connected converter under weak grids," *IEEE Transactions on Industrial Electronics*, vol. 70, no. 11, pp. 11310–11323, 2023.

[25] A. Mellit and S. A. Kalogirou, "Artificial intelligence techniques for photovoltaic applications: a review," *Progress in Energy and Combustion Science*, vol. 34, no. 5, pp. 574–632, 2008.

[26] B. Wang, Y. Zhang, and W. Zhang, "A composite adaptive fault-tolerant attitude control for a quadrotor UAV with multiple uncertainties," *Journal of Systems Science and Complexity*, vol. 35, no. 1, pp. 81–104, 2022.

[27] A. Moeed Amjad and Z. Salam, "A review of soft-computing methods for harmonics elimination PWM for inverters in renewable energy conversion systems," *Renewable and Sustainable Energy Reviews*, vol. 33, pp. 141–153, 2014.

[28] Y.-H. Liu, C.-L. Liu, J.-W. Huang, and J.-H. Chen, "Neural-network-based maximum power point tracking methods for photovoltaic systems operating under fast changing environments," *Solar Energy*, vol. 89, pp. 42–53, 2013.

[29] X. Lin, Y. Liu, J. Yu, R. Yu, J. Zhang, and H. Wen, "Stability analysis of three-phase grid-connected inverter under the weak grids with asymmetrical grid impedance by LTP theory in time domain," *International Journal of Electrical Power and Energy Systems*, vol. 142, no. 2022, Article ID 108244, 2022.

[30] W. Deng, Y. Zhang, Y. Tang, Q. Li, and Y. Yi, "A neural network-based adaptive power-sharing strategy for hybrid frame inverters in a microgrid," *Frontiers in Energy Research*, vol. 10, 2023.

[31] H. Mahamudul, M. Saad, and M. Ibrahim Henk, "Photovoltaic system modeling with fuzzy logic based maximum power point tracking algorithm," *International Journal of Photoenergy*, vol. 2013, Article ID 762946, 10 pages, 2013.

[32] Y. Duan, Y. Zhao, and J. Hu, "An initialization-free distributed algorithm for dynamic economic dispatch problems in microgrid: modeling, optimization and analysis," *Sustainable Energy, Grids and Networks*, vol. 34, Article ID 101004, 2023.

[33] B. Wang, D. Zhu, L. Han, H. Gao, Z. Gao, and Y. Zhang, "Adaptive fault-tolerant control of a hybrid canard rotor/wing uav under transition flight subject to actuator faults and model uncertainties," *IEEE Transactions on Aerospace and Electronic Systems*, vol. 59, no. 4, pp. 4559–4574, 2023.

[34] C.-L. Liu, J.-H. Chen, Y.-H. Liu, and Z.-Z. Yang, "An asymmetrical fuzzy-logic-control-based MPPT algorithm for photovoltaic systems," *Energies*, vol. 7, no. 4, pp. 2177–2193, 2014.

[35] H. Abu-Rub and A. Iqbal, "Quasi-Z-source inverter-based photovoltaic generation system with maximum power tracking control using ANFIS," *IEEE Transactions on Sustainable Energy*, vol. 4, no. 1, pp. 11–20, 2013.

[36] Q. Gu, S. Li, W. Gong, B. Ning, C. Hu, and Z. Liao, "L-SHADE with parameter decomposition for photovoltaic modules parameter identification under different temperature and irradiance," *Applied Soft Computing*, vol. 143, Article ID 110386, 2023.

[37] N. Priyadarshi, "Internet of things augmented a novel PSO-employed modified zeta converter-based photovoltaic maximum power tracking system: hardware realisation," *IET Power Electronics*, vol. 13, no. 13, pp. 2775–2781, 2020.